AISTech 2009 Steelmaking Conference Proc., (St. Louis, MO, May 4-7, 2009),
Assoc. Iron Steel Tech., Warrendale, PA, Vol. 1, 2009

Utilization of CON1D at ArcelorMittal Dofasco's No. 2 Continuous Caster for Crater End Determination

Joydeep Sengupta
Global R&D Hamilton
ArcelorMittal Dofasco, Inc.
Box 2460, 1330 Burlington Street East
Hamilton, Ontario, L8N 3J5 Canada
Phone – (905) 548-4739
Fax – (905) 548-4653

Manh-Kha Trinh
Steelmaking Technology
ArcelorMittal Dofasco, Inc.
Box 2460, 1330 Burlington Street East
Hamilton, Ontario, L8N 3J5 Canada
Phone – (905) 548-3005

David Currey
Global R&D Hamilton
ArcelorMittal Dofasco, Inc.
Box 2460, 1330 Burlington Street East
Hamilton, Ontario, L8N 3J5 Canada
Phone – (905) 548-4747

Brian G. Thomas
Dept. of Mechanical Science and Engineering
University of Illinois at Urbana-Champaign
1206 West Green Street
Urbana, IL 61801 USA
Phone – (217) 333-6919
Fax – (217) 244-6534

Key Words: Continuous Casting, Heat Transfer Analysis, Metallurgical Length

INTRODUCTION

Accurate determination of the position of final solidification point or *crater end* at ArcelorMittal Dofasco's No. 2 Continuous Caster (CC) is essential for maximizing both casting speed and equipment utilization. The caster is equipped with one 900-mm long, straight, water-cooled copper mold, and produces 218-mm thick slabs with a maximum width of ~1,600 mm. The casting speed range at the caster is presently ~1.0 – 1.7 m/min. The position of the crater end or caster *metallurgical length* is defined as the distance from the liquid steel meniscus to the point at which the strand becomes completely solid, as shown in **Figure 1** [1]. It is obvious that if the crater end extends beyond the machine length, the final portion of the partially solidified strand will no longer be supported by rolls on the strand broad faces. The ferrostatic pressure transmitted from the meniscus *via* the liquid pool and acting internally on the steel shell will then cause this unconstrained portion of strand to bulge out excessively. This will ultimately lead to a *whale formation* at the caster exit. To prevent extensive damage to the casting machinery, this catastrophic situation has to be avoided at all costs. In other words, the crater end must always be contained within the support roll segments under all casting conditions.

The metallurgical length of a caster is a complex function of steel grade, superheat, casting speed, intensity of mold and spray-water cooling, machine design, and strand dimensions [2]. Usually, an empirical parameter, known as the solidification constant, is used to determine the crater end position. The relationship is given by: $z_{CE} = \frac{V_c T^2}{4k^2}$ where z_{CE} = crater end position in mm, T = slab thickness in mm, V_c = casting speed in mm/min, and

k = average solidification constant for entire machine length in mm/min$^{0.5}$. The solidification constant varies considerably in the mold cooling and initial portion of the spray cooling zones, where the shell thickness changes rapidly with machine length. It then becomes fairly constant as the shell thickness growth slows down and solidification is eventually completed. For a typical slab caster similar to No. 2 CC design, the average value of k ranges from 25 to 28 mm/min$^{0.5}$, and is often provided by the CC OEM or determined by caster trials.

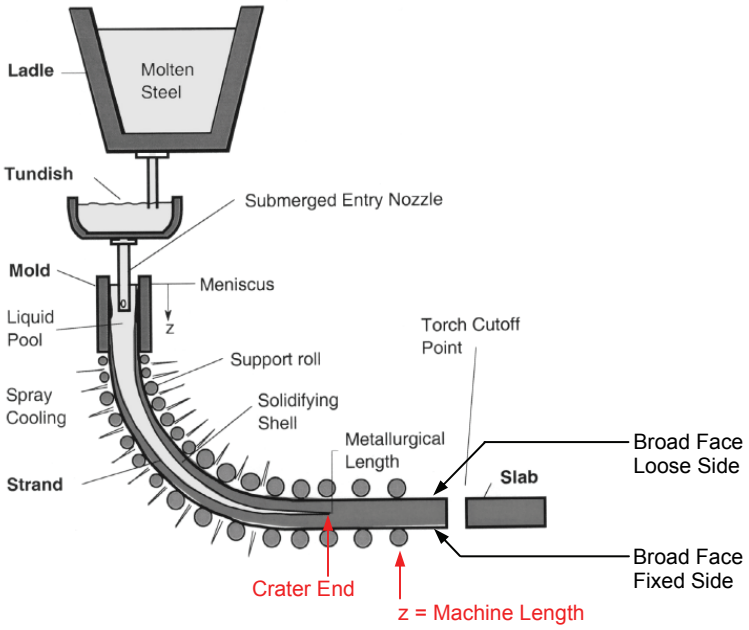

Figure 1: Schematic illustrating the crater end position or metallurgical length for a typical continuous caster [1].

Recently, No. 2 CC mold design was upgraded to achieve a casting speed of 2.0 m/min. A trial mold with design features almost similar to the improved design was installed at the caster to obtain temperature, heat flux and shell thickness data at higher casting speeds. It is assumed that the new molds will be at least as efficient as this trial mold. At higher casting speeds, the metallurgical length increases, *i.e.* crater end moves towards caster exit. Thus, there is a need to determine the crater end positions at speeds greater than 1.7 m/min for No. 2 CC. An average solidification constant can not be used to evaluate the risk of whaling at high speeds as this method is not robust, and does not take into account the variability of mold and spray-water cooling along the machine length. Quantification of realistic variation of heat transfer and shell thickness along the machine length depending on different casting conditions requires sophisticated computational heat transfer models that can predict the shell thickness and strand surface temperature with reasonable degree of accuracy. Therefore, ArcelorMittal's Global R&D Hamilton and ArcelorMittal Dofasco's Steelmaking Technology adopted this methodology to quantify the variation of crater end position with casting speed for No. 2 CC.

Towards this goal, a 1-D heat transfer and solidification model (CON1D) developed at the University of Illinois at Urbana-Champaign (UIUC) by Prof. Brian G. Thomas and his research group, was used in this study. However, a thorough validation work was required at the caster before the model could be utilized for evaluating the risk of whale formation at high casting speeds. CON1D was validated using No. 2 CC heat transfer data (for predictions related to mold cooling), and infra-red camera measurements (for predictions related to spray-water cooling). *Shim drop* trials conducted at various speeds to confirm shell thickness predictions. This paper summarizes the validation work carried out at ArcelorMittal Dofasco to facilitate the utilization of CON1D at No. 2 CC.

BRIEF DESCRIPTION OF CON1D DEVELOPED AT UIUC

CON1D is a FORTRAN program which models heat transfer and solidification in the mold region of a continuous caster. The model simulates one-dimensional transient heat transfer-solidification in the steel shell coupled with 2-D steady-state heat conduction in the mold. Hence, the model is most easily applied to regions away from the corners

of the cross-section. The heat flux extracted from the solidified shell surface can either be supplied as a specified function of distance below the meniscus, or can be calculated using the interfacial model included in the program. The superheat can be treated in three different ways in the program: 1) calculating temperature in the liquid steel; 2) supplying a superheat flux profile as a stepwise linear function of distance below the meniscus; or 3) letting the program calculate the heat flux added to shell surface, based on previous 3-D turbulent flow calculations. The program can simulate wide/narrow face, outer/inner face of molds (with or without curvature). It is also capable of calculating heat transfer as the strand passes by each roll in the spray zones beneath the mold.

The model features user-friendly input of the following comprehensive list of variables affecting mold heat transfer, (reasonable defaults are provided for many of these):

1) Complete mold geometry: water slots and bolts, mold curvature, mold plate design: variable thickness distribution and conductivity down mold, scale buildup on water channels, etc.
2) Mold flux properties and adjustable parameters: temperature-dependent viscosity and conductivity, variable slag rim thickness down mold, powder consumption rate, solid flux velocity, etc.
3) Temperature and composition-dependent properties of steel, copper, and water: thermal conductivity, specific heat, density, steel phase (austenite or ferrite), latent heat, solidus and liquidus temperatures, water inlet temperature, velocity, and pressure.
4) Oscillation mark size, frequency and stroke: effect on heat flow and mold flux consumption.
5) Effect of fluid flow on superheat delivery to the shell: enhanced thermal conductivity in the liquid, specified superheat flux to the solidifying interface, and model predicted superheat flux (slab casters).
6) Spray zone variables: hear transfer coefficient model, roll space, roll radius, contact angle, and nozzle spray width and length, and water flow rate.

The CON1D output (a typical example is shown in **Figure 2**) results include the following variables (as a function of distance below the meniscus):

1) Temperatures: mold hot face, cold face, shell surface and shell interior, cooling water
2) Shell thickness (including positions of liquidus, solidus, and shell isotherms);
3) Heat flux leaving the shell (across the interfacial mold / shell gap);
4) Ideal mold taper (based on 1D shrinkage calculations);
5) Thickness and velocity of solid and liquid flux layers in the mold/shell interfacial gap.

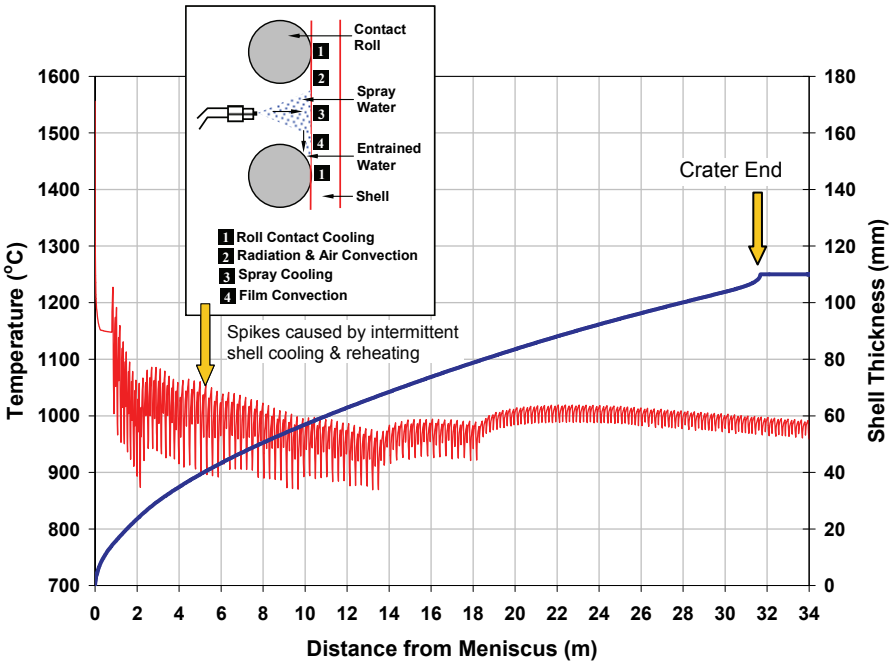

Figure 2: Plot showing CON1D-predicted shell surface temperature and thickness along the No. 2 CC machine length for a typical low carbon aluminum killed (LCAK) grade. The crater end is at ~32 m from meniscus.

For further details on CON1D and description of thermal boundary conditions, please refer to [3] and [4].

PRIMARY COOLING BY No. 2 CC MOLD

Heat flux removal and thermocouple data was obtained from a ~1,300-mm wide No. 2 CC mold under steady state casting conditions to test the performance of CON1D at speeds ranging from 1.0 to 1.6 m/min. A typical low carbon grade representing ~50 % of No. 2 CC's LCAK product mix was considered for this study. The casting process was assumed to attain steady state if the casting speed and mold width remained constant for at least 20 minutes and the standard deviation of heat flux data did not exceed 100 W/m^2. Compressed Level I data at one-second time intervals was used for time-averaging of heat transfer data during this steady state period.

Appropriate values of mold copper thickness, mold coating thickness, taper, slot design, water flow rates, water inlet temperature and pressure, and superheat were used as input information for CON1D. Appropriate thermophysical properties were calculated by CON1D for the heat transfer analysis. The computed liquidus temperature, thermal conductivity and specific heat data matched ArcelorMittal Dofasco's calculations closely. A heat flux vs. distance from meniscus curve obtained from OEM was used as an input thermal boundary condition – refer to **Figure 3(a)**. This curve was fine-tuned at different speeds to match the measured average heat removal data with CON1D predictions, as shown in **Figure 3(b)**. The heat flux removed at a location ~25 mm below the meniscus was estimated to be ~70% higher than the average heat flux extracted by the mold.

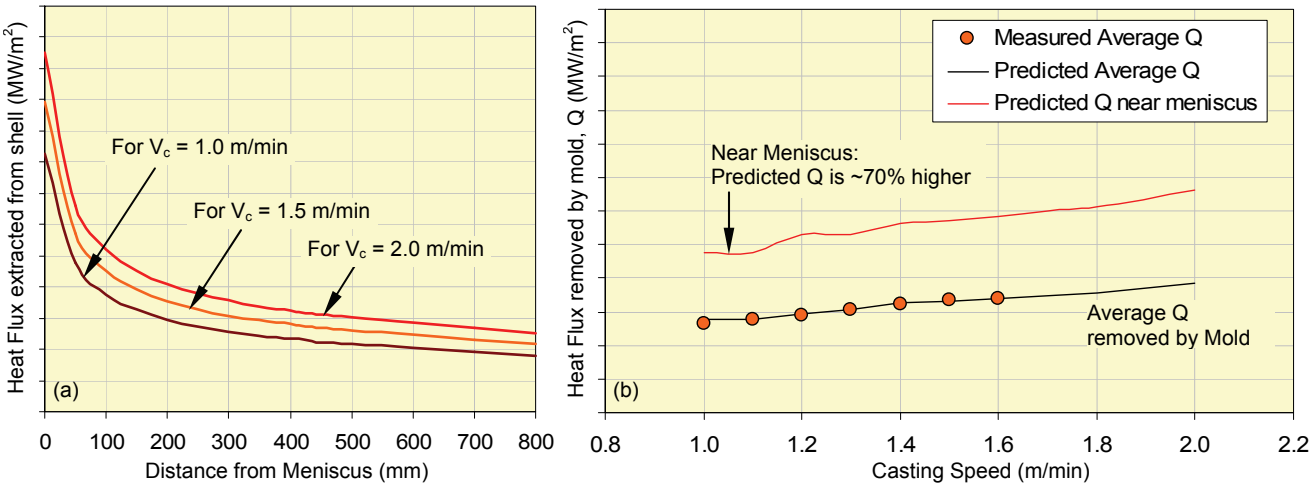

Figure 3: (a) Heat flux curves used by CON1D as input thermal boundary condition and (b) comparison between measured average heat flux removal data from a ~1,300-mm wide No. 2 CC mold and CON1D-predicted values at different speeds. The heat flux removed near the meniscus (~25 mm below) as predicted by CON1D is also shown.

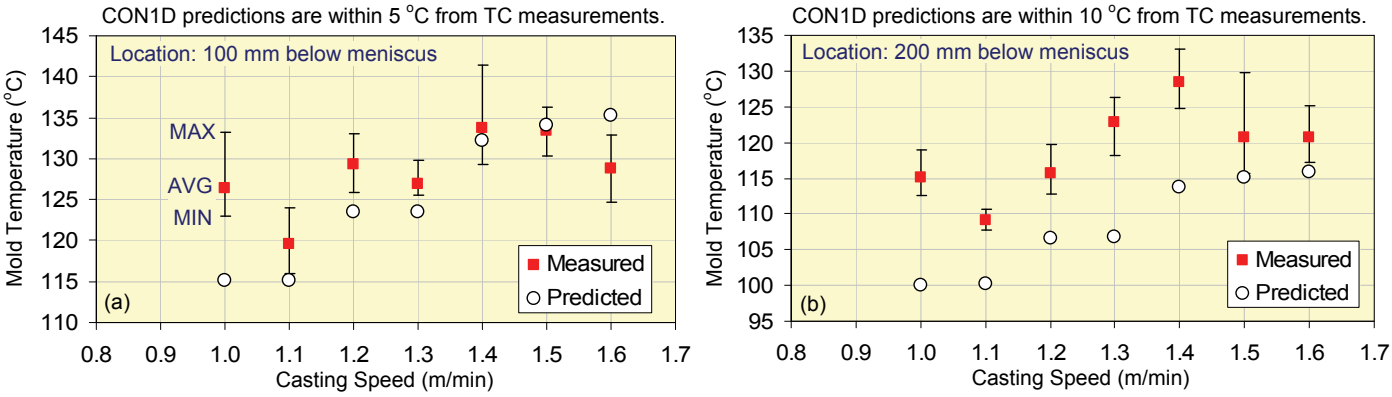

Figure 4: Comparison between thermocouple data obtained from four locations close to the fixed side broad face center of a ~1,300-mm wide mold at a distance of (a) 100 mm and (b) 200 mm below meniscus and CON1D predictions at different speeds. The thermocouples were located ~20 mm from the mold hot face.

Once a match between measured and predicted heat flux removal data was obtained, temperature data obtained from thermocouples embedded into the mold broad faces (for Breakout Detection System) was compared with predicted values at locations 100 and 200 mm below the meniscus. Referring to **Figure 4**, it can be concluded that the CON1D predictions are very close (*i.e.* within 5 – 10 ^{o}C) to plant data and its performance was found to be satisfactory.

For further model validation, shell thickness measurements, obtained from a ~1,000-mm wide HSLA slab cast at ~1.1 m/min, were compared with CON1D predictions. The shell thickness was measured at the center of broad and narrow faces using Baumann-type sulphur prints generated from etched slab samples. To improve the clarity of the macrographs and accuracy of the shell thickness measurements, additional sulphur was introduced into the No. 2 CC for a short time period. To extract shell thickness data from CON1D, a solid fraction, $f_s = 0.7$ was used. **Figure 5** summarizes the results from this study. Referring to **Figure 5(a)**, it can be concluded that beyond a distance of ~300 mm from the meniscus, CON1D predicts the shell thickness very well. The slight mismatch observed between 0 – 300 mm can be attributed to the interference of the submerged entry nozzle (SEN) in the heat extraction process, which is not considered by the boundary condition formulations within CON1D.

Referring to **Figure 5(b)**, which shows the narrow face shell thickness data, an opposite effect can be observed. CON1D predictions are close to the measured data only up to a distance of ~300 mm from the meniscus. Based on CFD model calculations performed at ArcelorMittal Dofasco, the metal jet exiting the SEN impinges upon the narrow face at a distance of ~300 – 350 mm below the meniscus. Thus, the mismatch can be explained by the *shell thinning effect* caused by the impingement of the metal jet on the narrow face shell. Again, this effect is not considered in the CON1D calculations. To rectify this error, a solid fraction, $f_s = 1.0$ is recommended for locating the shell thickness on the narrow faces.

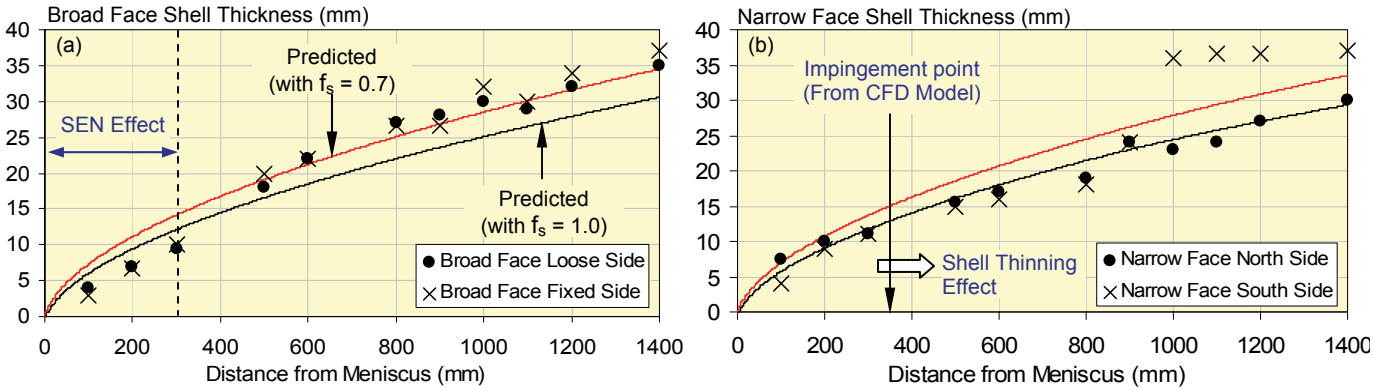

Figure 5: Comparison between shell thickness data obtained from (a) broad faces and (b) narrow faces of a ~1,000-mm wide mold at V_c = 1.1 m/min, and CON1D-predicted results. The steel grade is a typical HSLA.

SECONDARY COOLING BY No. 2 CC SPRAY WATER ZONES

A *quick-win* collaboration was established with ArcelorMittal Dofasco's Hot Mill Technology to utilize Hot Mill's extensive experience in measuring hot band surface temperatures using infrared cameras, and to extend this thermal imaging technique to No. 2 CC. A trial was conducted at the caster to obtain steady state casting conditions at speeds ranging from 1.4 to 1.7 m/min. Strand temperature data was continuously recorded on a data acquisition system using a factory-calibrated camera. Unlike pyrometers, the infrared camera was quickly installed at an accessible location near the caster exit, and thus, a shutdown for installation was not required. Two additional cameras were used to cross-check the calibration and camera settings. The results are shown in **Figure 6**. Relevant snapshots were post-processed to obtain steady-state surface temperature at the broad face center near the caster exit, as shown in **Figure 7(a)** and **(b)**. CON1D simulations were set up using appropriate process parameters. Finally, the CON1D temperature predictions were compared with the measurements, and as shown in **Figure 7(c)**, a reasonable agreement was obtained at four different casting speeds.

To determine the shell thickness developed in the spray cooling zone, *shim drop* trials [5] were carried out at the caster at three different speeds: 1.6, 1.7 and 1.8 m/min. During these trials, ~25 mm wide and ~6 mm thick shims were dropped on the broad face of the strand at a location close to the unbending segment exit. The shim moved forward along with the strand, and a surface indentation was created, as shown in **Figure 8(a)**, due to compressive forces generated by the support rolls on the strand broad faces. This action effectively simulates a 6-mm roll misalignment and an artificial mid-way crack is expected to occur near the solidification front. The location of the mid-way crack (assuming this occurs at $f_s = 0.7$) from the strand centerline can then be used to determine the slab thickness at the machine length corresponding to the shim drop location at the caster.

To locate the mid-way crack, two longitudinal samples were collected from the slab that contained the shim-drop indentations. These samples were milled and ground, heat-treated and then etched repeatedly with diluted cupric ammonium chloride solution until the primary dendritic structure was revealed, as shown in **Figure 8(b)**. The slab thickness, T, and centerline location were obtained from the reference sample. The midway crack was also located on the shim-drop sample, also shown in the figure. The average distance of the mid-way crack from the bottom edge of the sample (fixed side), z, was determined from ten measurement points. Thus, the shell thickness is given by the relationship: $t = T - z$.

To compute the shell thickness at the shim-drop location, CON1D simulations were set up for the appropriate casting conditions prevailing during the trials. A comparison between the measured and predicted shell thickness is presented in **Figure 8(c)**. From this data, it can be concluded that CON1D predictions matched shell thickness measurements fairly well.

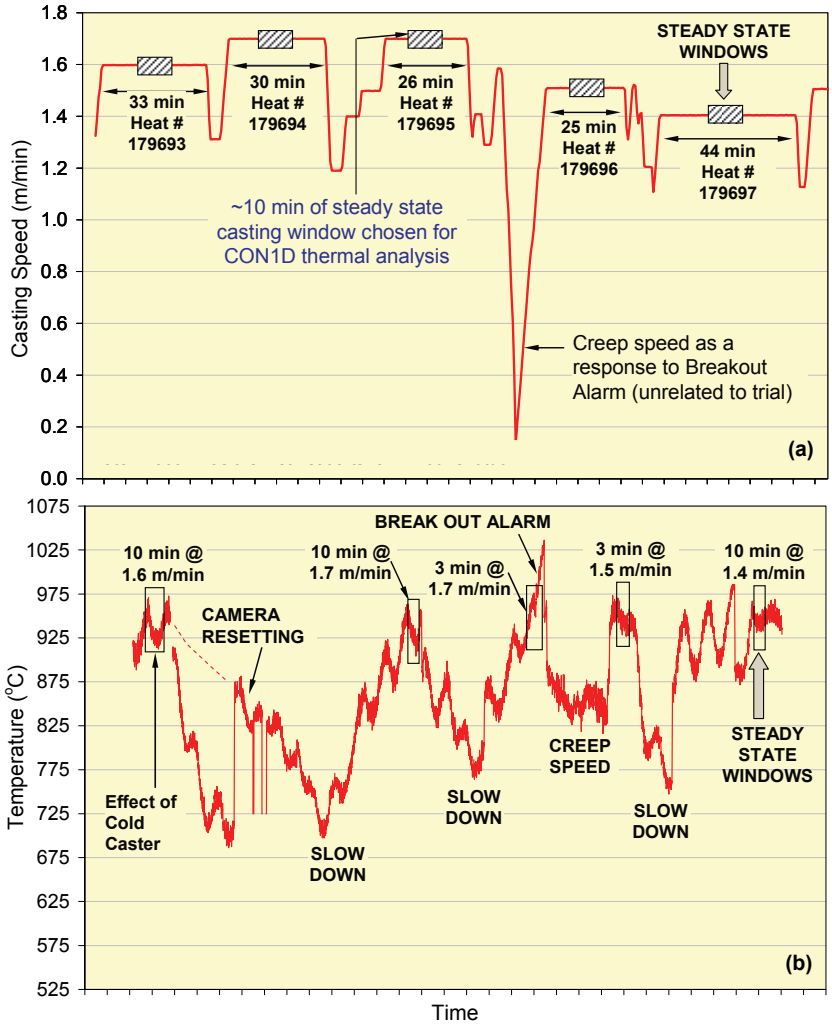

Figure 6: (a) Variation of casting speed with time recorded during the infrared camera trial and (b) variation of strand surface temperature at the center of strand broad face recorded by the infrared camera during the same time period. Steady-state windows were chosen at various speeds for time-averaging of temperature data.

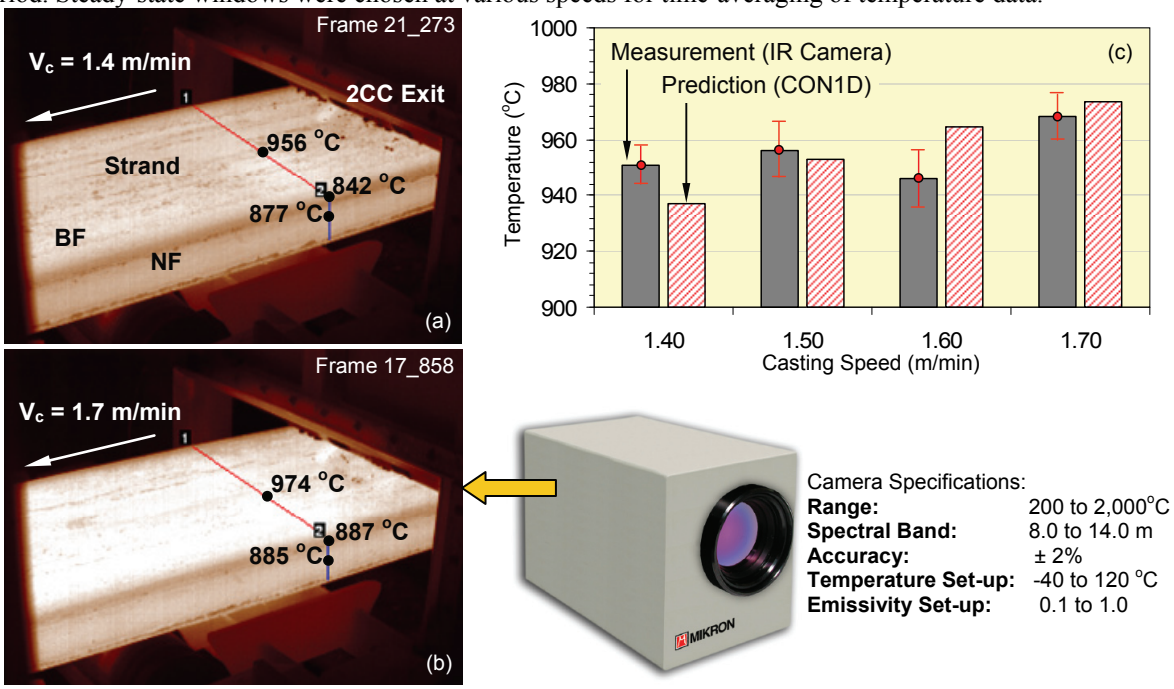

Figure 7: Snapshots from video recorded by the infrared camera (bottom right) during the trial. Surface temperatures near No. 2 CC Exit at (a) 1.4 m/min and (b) 1.7 m/min are shown. Temperature data can be extracted from any pixel on a frame-of-interest, using software provided by Mikron Infrared, Inc., and (c) comparison between measured and predicted surface temperatures of the broad face center indicated a good agreement (within ~2%).

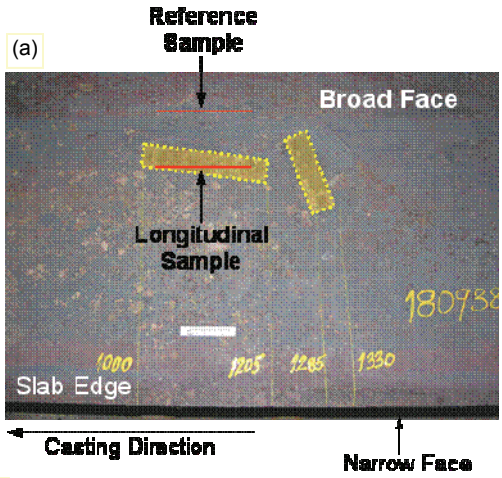

(c)

Speed (m/min)	Shell Thickness (mm)	
	Measured	Predicted
1.6	90.1	84.1
1.7	87.3	81.4
1.8	77.0	79.1

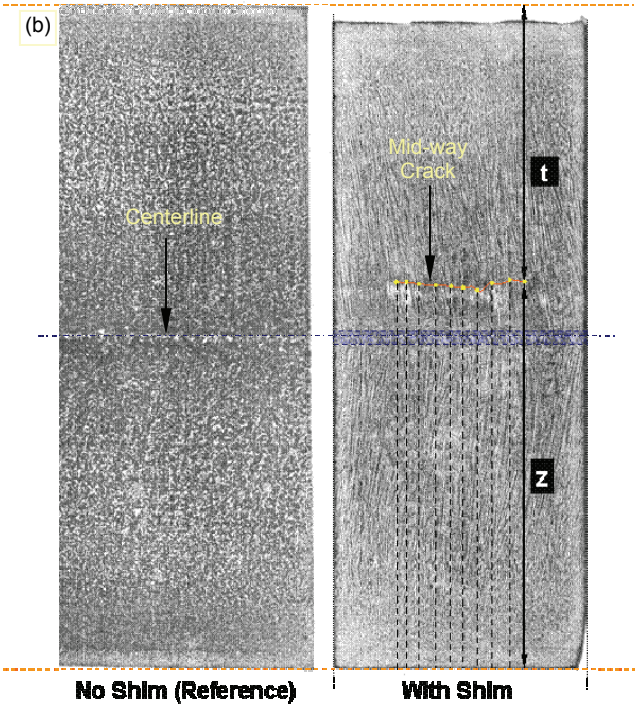

Figure 8: (a) Location of indentations on the slab broad face (in yellow) showing the position of the 6-mm thick shims dropped on the strand at a distance of ~18 m from the meniscus (near the unbending segment exit).

Longitudinal slab samples were obtained from locations below the indentation and away from it (reference sample) for etching. (b) Etched and inked macrographs for the reference and shim-drop samples were used to locate the slab centerline and location of the mid-way crack created by the shim from the bottom edge of the sample (fixed side).

CRATER END PREDICTIONS FOR No. 2 CC

Based on the validation work on CON1D completed at No. 2 CC, as described in the previous sections, it was concluded that the heat transfer model can now be utilized for predicting the metallurgical length in the machine at different casting speeds with a reasonable degree of accuracy. **Figure 9** shows the variation of crater end location at 1.6, 1.7 and 1.8 m/min (same casting conditions corresponding to the shim drop trial cases) for a typical LCAK steel grade. It is evident that the crater end is well contained by the support rolls at these speeds. The average solidification constant for the machine at these speeds was determined to be ~26.5 mm/min$^{-0.5}$.

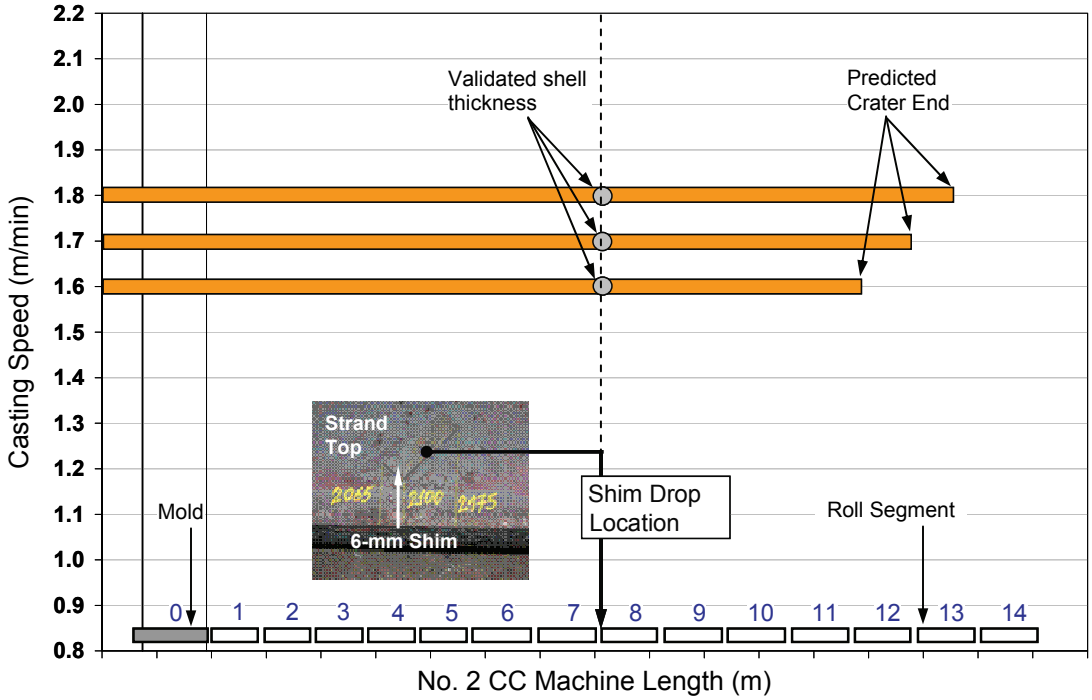

Figure 9: Plot showing crater end locations predicted by CON1D along No. 2 CC machine length. The location of shim drop trials is also indicated. Shell thickness predictions from CON1D were validated at this machine length.

However, the reader is reminded that these predictions are for steady state casting conditions wherein the casting speed and width are not changed at the caster. However, as mentioned earlier, the metallurgical length can vary with grade chemistry, superheat, and heat transfer conditions. To determine the variation of crater end position under variable casting conditions, a parametric study was conducted using CON1D to study the effect of variations in steel chemistry, superheat, mold copper thickness wear, and plugged water spray nozzles. The result is summarized in **Table I**. Based on this study; a tolerance of +1.0 m was imposed on the CON1D predicted metallurgical length to account for the variability in casting conditions.

CONCLUDING REMARKS

This technical work carried out at ArcelorMittal Dofasco demonstrates the utilization of sophisticated modeling tools, such as, CON1D, for obtaining useful quantitative predictions related to the casting process (*e.g.* crater end location). These tools are particularly helpful if a process parameter is very difficult to be measured directly or require installation of expensive instrumentation at the caster. However, application of these models requires thorough validation work, using plant data that is obtained from Level I/II or caster trials (*e.g.* temperature and shell thickness) as described in this study. The CON1D-predicted metallurgical length at high casting speeds will be used to review the equipment design and spray water cooling conditions for No. 2 CC to minimize the risk of whale

formation. Further work is still required to achieve this goal. Firstly, pyrometers are required to be installed at the caster to validate surface temperature predictions at locations closer to the unbending segments. This will allow quantification of cooling intensity of current spray water practices at No. 2 CC that are used at different speeds. The practices can then be modified to ensure crater end containment at all casting speeds. Secondly, the effect of unsteady state casting conditions, such as speed and width changes, on metallurgical length is yet to be determined. This will require modification of the FORTRAN code residing within CON1D to simulate these casting events. Additional caster trials may be required for validating these changes to the model. Efforts are continuing at ArcelorMittal Dofasco to meet these goals and to improve the accuracy of metallurgical length predictions for No. 2 CC.

Table I: Comparison between CON1D predicted metallurgical length at 1.8 m/min under steady state casting conditions and steady state casting conditions with process variability.

Casting Conditions	**Predicted Metallurgical Length (m) Vc = 1.8 m/min & Grade: LCAK**
Steady state casting with following conditions: - No Speed and Width changes - Aim Grade Chemistry - Aim Superheat - New Mold Copper Plates - No Spray Nozzle Plugging	31 m approx.
Steady state with following conditions: - No Speed and Width changes - Grade Chemistry with max for every element (Lowest Liquidus and Solidus Temperatures) - Max Superheat allowed per SOP - Scrap Mould Thickness (max variation in mold cooling) - Max Spray Nozzle Plugging (max variation in spray cooling)	32 m approx

ACKNOWLEDGEMENTS

The authors would like to thank ArcelorMittal Dofasco's Steelmaking Operations, Maintenance and Technology, especially Dave Arnott (No. 2 CC Day Operations Support) and Norbert Strobl (No. 2 CC Technology Coordinator), for their continuous support during the caster trials – in addition to the technical advice and practical knowledge they shared with the authors. Contributions from ArcelorMittal Global R&D's Jim Casey and Alex Cavicchioli (for developing etched macrographs) and ArcelorMittal Dofasco Hot Mill Technology's Kevin Hunt (for providing the infrared camera, data acquisition software, and technical support during caster trials) are also gratefully acknowledged by the authors.

REFERENCES

[1] B. G. Thomas, "Modeling of Continuous Casting", *Making, Shaping and Treating of Steel*, 11th Edition, Vol. 5, Casting Volume, AISE Steel Foundation, Pittsburgh, PA, 2003, pp. 5.1-5.24.
[2] K. Schwerdtfeger, "Heat Withdrawal in Continuous Casting of Steel", *Making, Shaping and Treating of Steel*, 11th Edition, Vol. 5, Casting Volume, AISE Steel Foundation, Pittsburgh, PA, 2003, pp. 4.1-4.41.
[3] B. G. Thomas, *CON1D Users Manual Version 8.0*, UIUC Continuous Casting Report, 2004.
[4] Y. Meng, *Modeling Interfacial Slab Layer Phenomena in the Shell / Mold Gap in Continuous Casting of Steel*, Ph.D. Thesis, University of Illinois, August, 2004.
[5] R.H. Merk, M. Vigon and S. Ingham, "Improved Productivity and Quality at Stelco's LE Steel Caster", *McMaster Symposium on Iron & Steelmaking*, McMaster University Publication, No. 30, April - May 2002, pp. 161-173.